# Exciton spin coherence and electromagnetically induced transparency in the transient optical response of GaAs quantum wells

Mark C. Phillips* and Hailin Wang
*Department of Physics and Oregon Center for Optics, University of Oregon, Eugene, Oregon 97403, USA*
(Received 9 July 2003; revised manuscript received 30 October 2003; published 30 March 2004)

We report experimental studies of electromagnetically induced transparency (EIT) arising from exciton spin coherence in the transient optical response of GaAs quantum wells. The exciton spin coherence, which is a direct result of Coulomb correlations between excitons with opposite spins, is induced via bound or unbound two-exciton states. Theoretical analyses based on a three-level model illustrate the manifestation of EIT in a transient regime and provide qualitative guidance for understanding the transient behaviors observed in the EIT experiments. Additional studies of the effects of exciton energy renormalization on optical Stark splitting also provide insights on how exciton many-body interactions can lead to unusual time-dependent asymmetric EIT line shapes.

DOI: 10.1103/PhysRevB.69.115337 PACS number(s): 78.47.+p, 42.50.Gy, 42.50.Hz, 78.67.De

## I. INTRODUCTION

Coherent manipulation of nonradiative quantum coherences between states that are not directly dipole coupled can lead to a variety of remarkable coherent nonlinear optical phenomena.[1–3] Destructive interference induced by nonradiative coherences in a three-level system can render an otherwise opaque medium nearly transparent, leading to electromagnetically induced transparency (EIT).[4,5] Other closely related phenomena include lasing without inversion,[6–8] stimulated Raman adiabatic passage,[9,10] and slow light[11,12] and stopped light.[13,14] The tremendous success in exploiting nonradiative coherences in atomic systems has stimulated great interest in extending these studies to semiconductors,[15–29] for the understanding of quantum coherences in semiconductors and also for potential applications of these phenomena.

There are two major obstacles for coherent manipulation of quantum coherences in semiconductors. First of all, with the exception of electron-spin coherence,[30,31] quantum coherences in semiconductors are extremely fragile against dynamic processes such as exciton-exciton and exciton-phonon scattering.[32] The resulting rapid decoherence necessitates that coherent manipulation be carried out in a transient regime. By employing ultrafast optical pulses, one can generate the large Rabi frequency (which sets the characteristic time scale for coherent manipulation) necessary to overcome the rapid decoherence. The use of ultrafast pulses, however, also limits the coherent interaction time. As will be discussed in this paper, the realization and manifestation of EIT in the transient regime can differ considerably from that in a steady-state limit or in an adiabatic limit.

Second, the many-body Coulomb interactions inherent to semiconductors greatly complicate and in many instances profoundly affect coherent nonlinear optical processes.[33–48] Under properly designed conditions, however, these interactions can also be exploited for the generation and manipulation of quantum coherences, as we will discuss in detail in this paper. In this regard, coherent nonlinear optical phenomena such as EIT also provide a powerful tool to reveal the intricate relations between quantum coherences and many-body Coulomb interactions.

We have exploited Coulomb correlations between excitons with opposite spins to induce exciton spin coherence, which would not exist in the absence of the many-body correlations. In this paper, we present studies of EIT arising from the exciton spin coherence in the transient optical response in GaAs semiconductor quantum wells (QW's). Experimental demonstration of EIT from the exciton spin coherence has been reported in an earlier study.[49] The primary aim of this paper is to address the manifestation of EIT in a transient regime and how many-body Coulomb interactions both induce and also complicate the transient EIT process. The paper is organized as follows. In Sec. II, we discuss the conditions and behaviors of EIT in the transient optical response in which the adiabatic condition is not satisfied. The discussions are based on numerical solutions to the density-matrix equations for a three-level system. In Sec. III, we present detailed experimental studies on the transient behavior of EIT induced by exciton spin coherence via bound and unbound two-exciton states in GaAs QW's. In Sec. IV, we present additional studies on effects of exciton-exciton interactions on optical Stark splitting of excitons. These additional studies provide important physical insight for understanding the asymmetric EIT line shape observed in our experimental study. Section V presents a summary.

## II. EIT IN A TRANSIENT REGIME

EIT is a phenomenon whereby an optical transition in a multilevel system can be made nearly transparent due to destructive quantum interference. For simplicity, here we will consider a $\Lambda$-type three-level system with no inhomogeneous broadening. While theoretical analyses based on the atomic-like three-level model do not provide an adequate description for EIT in semiconductors, these analyses illustrate important conditions for realizing EIT in a transient regime and also reveal unusual transient behaviors of EIT, as we discuss in detail in this section.

As shown in Fig. 1, the $\Lambda$ configuration consists of two lower states $|a\rangle$ and $|b\rangle$ which are both dipole coupled to an upper state $|e\rangle$. States $|a\rangle$ and $|b\rangle$ are not dipole coupled, but can be coupled via a two-photon transition. EIT can be observed in this system when two optical fields $\mathcal{E}_a$ and $\mathcal{E}_b$ reso-

 

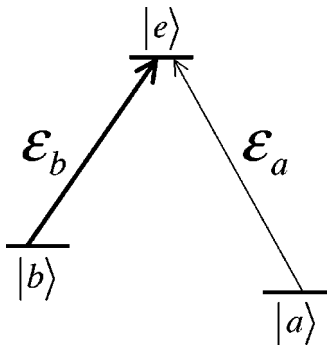


FIG. 1. Schematic of EIT scheme for a $\Lambda$-type three-level system.

nant or nearly resonant with the two dipole optical transitions are applied. In this case, a special coherent superposition of states $|a\rangle$ and $|b\rangle$ can lead to a cancellation of the optical absorption. For resonant optical fields, this so-called dark state is given by

$$|\psi\rangle_{NC}=\Omega^{-1}[\Omega_b|a\rangle-\Omega_a|b\rangle], \tag{1}$$

where $\Omega=(\Omega_a^2+\Omega_b^2)^{1/2}$, and $\Omega_{a(b)}$ is the Rabi frequency for the $|a\rangle\leftrightarrow|e\rangle$ ($|b\rangle\leftrightarrow|e\rangle$) dipole transition. This dark state maximizes the destructive interference between the two absorption pathways to state $|e\rangle$.

In typical EIT experiments in atomic systems, the system is either adiabatically pumped into the dark state or else evolves into the dark state in the steady-state limit. The destructive quantum interference underlying EIT, however, occurs even when the system is only partially in the dark state. Here, we will explore how coherent superpositions of states $|a\rangle$ and $|b\rangle$, i.e., nonradiative coherences, can be induced and controlled in a transient regime and how these transient nonradiative coherences can lead to induced transparency in optical absorption spectra.

We assume applied electric fields $\mathcal{E}_a$ and $\mathcal{E}_b$ with

$$\mathcal{E}_a(t)=\tfrac{1}{2}E_a(t)e^{-i\nu_a t}+\text{c.c.}, \tag{2}$$

$$\mathcal{E}_b(t)=\tfrac{1}{2}E_b(t)e^{-i\nu_b t}+\text{c.c.}, \tag{3}$$

where $\mathcal{E}_a$ is a weak probe field with center frequency $\nu_a$ and pulse envelope $E_a(t)$, applied to the $|a\rangle\leftrightarrow|e\rangle$ transition. We make no restriction on the magnitude of the pump field $\mathcal{E}_b$, which has center frequency $\nu_b$ and pulse envelope $E_b(t)$, and is applied to the $|b\rangle\leftrightarrow|e\rangle$ transition. For convenience, we will refer to the applied fields in terms of their Rabi frequencies $\Omega_a(t)=\mu_a E_a(t)/\hbar$ and $\Omega_b(t)=\mu_b E_b(t)/\hbar$, where $\mu_a$ and $\mu_b$ are the dipole transition matrix elements (taken to be real for convenience).

We take state $|a\rangle$ to be the ground state, with states $|b\rangle$ and $|e\rangle$ initially unoccupied. Therefore, to zeroth order in $\Omega_a$, $\rho_{aa}^{(0)}=1$, where $\rho_{aa}$ is the population in state $|a\rangle$ with the total population of the system normalized to one, and all other terms are zero. Note that this is a direct consequence of states $|b\rangle$ and $|e\rangle$ being unoccupied in the absence of $\Omega_a$, so that $\Omega_b$ is pumping on an "empty" transition. This would not be the case for a *V*-type three-level system. To first order in $\Omega_a(t)$, and within the rotating wave approximation, the equations of motion for the density-matrix elements (in a rotating frame) are

$$\frac{\partial}{\partial t}\rho_{ea}^{(1)}(t)=(i\delta_a-\gamma)\rho_{ea}^{(1)}(t)+i\Omega_a(t)/2+i\Omega_b(t)\rho_{ba}^{(1)}(t)/2, \tag{4}$$

$$\frac{\partial}{\partial t}\rho_{ba}^{(1)}(t)=[i(\delta_a-\delta_b)-\gamma_{ab}]\rho_{ba}^{(1)}(t)+i\Omega_b(t)^*\rho_{ea}^{(1)}(t)/2. \tag{5}$$

The matrix element $\rho_{ea}^{(1)}(t)$ describes the dipole coherence between states $|a\rangle$ and $|e\rangle$, while $\rho_{ba}^{(1)}(t)$ describes the nonradiative coherence between states $|a\rangle$ and $|b\rangle$. The decoherence rates for the dipole and nonradiative coherences are given by $\gamma$ and $\gamma_{ab}$, respectively. The detunings of the applied fields are given by $\delta_a=\nu_a-\omega_a$ and $\delta_b=\nu_b-\omega_b$, where $\omega_a$ and $\omega_b$ are the resonance frequencies for the two dipole transitions.

We solved the above coupled differential equations numerically using a fourth-order Runge-Kutta routine. The applied pump and probe fields were assumed to have a Gaussian temporal envelope. The absorption spectrum of the probe pulse was calculated from the relationship $\alpha(\delta_a)\propto\text{Im}[\rho_{ea}^{(1)}(\delta_a)/\Omega_a(\delta_a)]$, where $\rho_{ea}^{(1)}(\delta_a)$ and $\Omega_a(\delta_a)$ are the Fourier transforms of $\rho_{ea}^{(1)}(t)$ and $\Omega_a(t)$, respectively. The resulting spectrum was normalized so that the peak value of the linear absorption (in the absence of the pump pulse) equaled one.

We can deduce some basic results from the form of the equations, even before considering the numerical solutions. First, in the absence of the nonlinear drive term $i\Omega_b(t)\rho_{ba}^{(1)}(t)/2$ in Eq. (4), the equation reduces to the linear response of a two-level system. Any changes to the probe absorption, therefore, are the direct result of the nonradiative coherence $\rho_{ba}^{(1)}(t)$. Second, the nonlinear drive term is also zero when the pump field $\Omega_b$ is zero, even though $\rho_{ba}^{(1)}(t)$ may still persist. A very short pump pulse effectively reduces the coherent interaction time. In the context of Eq. (4), EIT can be viewed as the result of destructive interference between the polarization induced by the probe and the polarization induced by both the pump and the nonradiative coherence.

The transient spectral response is obtained by applying a probe pulse with duration shorter than the dipole decoherence time, or in other words, with a spectral bandwidth larger than the absorption linewidth. In this case, the probe absorption is determined not only by the state of the system at the time of the probe pulse, but also by the temporal evolution of $\rho_{ea}^{(1)}(t)$ after the probe pulse. As can be seen from Eq. (4), once the nonradiative coherence is generated, it will continue to drive the dipole coherence $\rho_{ea}^{(1)}(t)$ as long as both $\rho_{ba}^{(1)}(t)$ and the pump field persists, even when the applied probe field is zero.

We consider a model EIT system in which the nonradiative decoherence rate is small: $\gamma_{ab}=0.01\gamma$. We take the probe duration (Gaussian full width) to be $0.1\gamma^{-1}$ and the

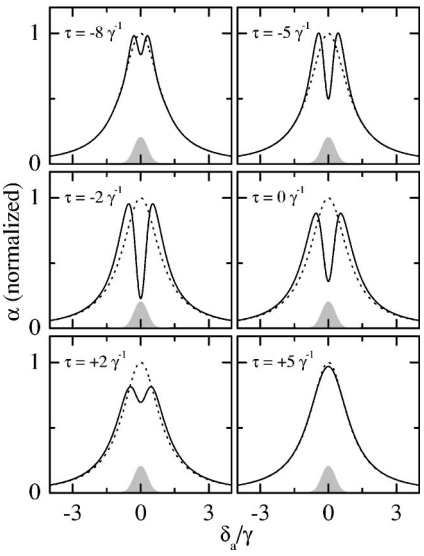


FIG. 2. Dependence of EIT on pump-probe delays. The solid (dotted) curves show the absorption spectra of the probe in the presence (absence) of the pump. The pump spectrum is shown as the shaded area. The pump and probe durations are $10\gamma^{-1}$ and $0.1\gamma^{-1}$, respectively, and the pump-probe delay $\tau$ is indicated in the figure. We also took $\Omega_b=\gamma$ and $\gamma_{ab}=0.01\gamma$.

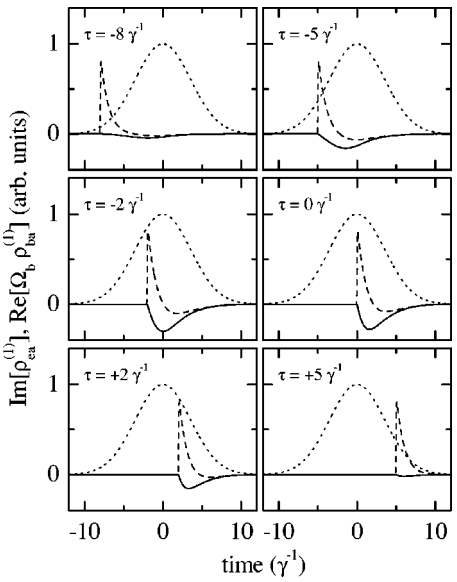


FIG. 3. Temporal evolution of the dipole and nonradiative coherences. The nonlinear driving term $\mathrm{Re}[\Omega_b(t)\rho_{ba}^{(1)}(t)]$ associated with the nonradiative coherence is shown as the solid curve, and the dipole coherence term $\mathrm{Im}[\rho_{ea}^{(1)}(t)]$ is shown as the dashed curve. The pump field envelope is shown as the dotted curve. The pump-probe delay $\tau$ is indicated in the figure and other conditions are the same as for Fig. 2.

pump duration to be $10\gamma^{-1}$. Figure 2 shows numerical solutions of the probe absorption spectrum under transient excitation conditions at various delays between the pump and probe pulses, and with $\delta_b=0$ and $\Omega_b=\gamma$. The absorption spectrum exhibits an EIT dip with a depth highly dependent on the pump-probe delay $\tau$ ($\tau>0$ indicates that the probe pulse arrives after the peak of the pump pulse). We note that the spectra are not symmetric about $\tau=0$. Instead, the EIT dip appears for large negative pump-probe delays, reaches a maximum depth when the probe slightly precedes the pump, and then disappears rapidly for positive delays.

We can gain additional insight into the behavior of the absorption spectra by considering the temporal evolution of $\mathrm{Im}[\rho_{ea}^{(1)}(t)]$ and $\mathrm{Re}[\Omega_b(t)\rho_{ba}^{(1)}(t)]$, plotted in Fig. 3 for the same conditions as in Fig. 2. Figure 3 shows that the maximum EIT signal is obtained when the nonlinear driving term $\mathrm{Re}[\Omega_b(t)\rho_{ba}^{(1)}(t)]$ is maximized during the decay of $\mathrm{Im}[\rho_{ea}^{(1)}(t)]$. This occurs when the probe slightly precedes the peak of the pump pulse. In this case, the nonradiative coherence can interact with the peak fields of the pump pulse.

Figures 4(a) and 4(b) illustrate the importance of a pump pulse which is long relative to the dipole decoherence time, where we plot the absorption spectrum for different pump durations $t_{pump}$, and with $\tau=-t_{pump}/2$. Other parameters including the peak pump intensity are the same as before. If the pump duration is too short, as in Fig. 4(a), then the EIT response is minimal. The pump duration must be long enough to allow the nonlinear drive term to influence the dipole coherence, leading to the EIT dip. In the spectral domain, the corresponding explanation is that the pump spectral bandwidth must be smaller than the absorption linewidth in order to observe a spectrally sharp EIT dip.

The sensitive dependence of EIT on the nonradiative coherence is exemplified by the behavior of the EIT dip as we vary the nonradiative decoherence rate. Figures 4(c) and 4(d) show absorption spectra for two different values of $\gamma_{ab}$, at fixed pump intensity and duration. A large $\gamma_{ab}$ inhibits the generation of a nonradiative coherence and there is no EIT dip present in the absorption spectra. In particular, the regime where $\gamma_{ab}\gg\gamma$ is equivalent to removing all coupling between the two dipole transitions. As $\gamma_{ab}$ decreases, the magnitude as well as the duration of the nonradiative coherence increases, and the EIT dip becomes more pronounced. However, decreasing $\gamma_{ab}$ below the pump spectral bandwidth has little additional effect on the absorption spectrum, as shown

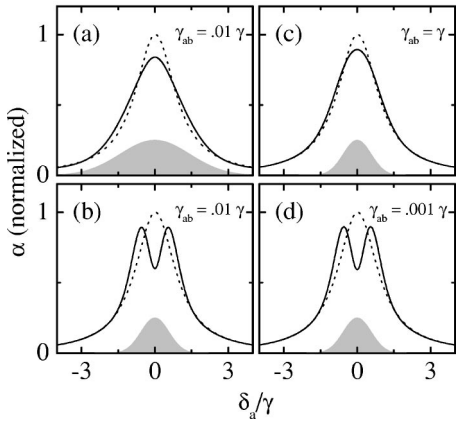


FIG. 4. Dependence of EIT on the pump duration and on the decay rate of the nonradiative coherence. For (a), $t_{pump}=2\gamma^{-1}$. For (b)–(d), $t_{pump}=5\gamma^{-1}$. In all cases, $\Omega_b=\gamma$.

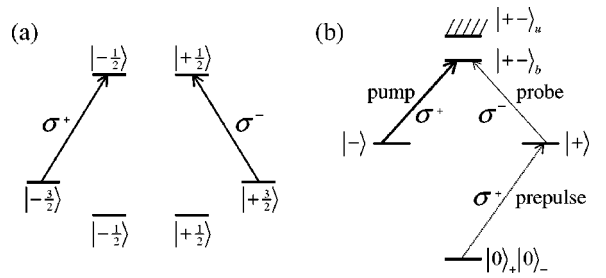


FIG. 5. (a) Schematic energy-level diagram for a GaAs quantum well, along with the circular polarization selection rules for the hh exciton transition. (b) EIT scheme using the bound two-exciton state. Energy levels shown are the *N*-exciton energy eigenstates, with ground state $|0\rangle_+|0\rangle_-$, one-exciton states $|+\rangle$ and $|-\rangle$, bound two-exciton state $|+-\rangle_b$, and unbound two-exciton states $|+-\rangle_u$.

in Fig. 4(d). In this case, the pump field amplitude reaches zero before the nonradiative coherence, and is therefore the limiting factor in the coherent nonlinear response.

The above theoretical analysis provides important guidance for understanding as well as designing transient experiments to realize EIT in semiconductors. While attaining the large Rabi frequency necessary to overcome rapid decoherence favors the use of very short pump pulses, the decoherence time for the relevant dipole coherence also sets a lower limit on the duration of the pump pulses that are suitable for the transient EIT experiment. In addition, in a somewhat counterintuitive way, the maximum destructive quantum interference and thus maximum EIT effects occur when the probe pulse slightly precedes the pump pulse. It should be added that transient behaviors of EIT in semiconductors are also strongly influenced by underlying many-body Coulomb interactions, as we discuss in detail in the following two sections.

## III. EIT INDUCED BY EXCITON SPIN COHERENCE

Our experimental studies to realize EIT in semiconductor QW's have exploited the use of exciton spin coherence. For semiconductors such as a GaAs QW, the interband optical transitions are characterized by excitonic transitions between the doubly degenerate conduction bands with $s=\pm 1/2$ and the doubly degenerate heavy-hole (hh) and light-hole (lh) valence bands with $j_z=\pm 3/2$ and $j_z=\pm 1/2$, respectively. For the hh excitonic transitions, spin-up $|+\rangle$ ($\sigma^+$ transition) and spin-down $|-\rangle$ ($\sigma^-$ transition) excitons can be excited with $\sigma^+$ and $\sigma^-$ circularly polarized light, respectively, as shown in Fig. 5(a). Although the $|+\rangle$ and $|-\rangle$ excitons share no common states, these excitons can interact with each other via Coulomb correlations, leading to the formation of bound and unbound two-exciton states (biexcitons), as shown by the *N*-exciton energy eigenstates in Fig. 5(b). Exciton spin coherence, i.e., coherent superposition of the $|+\rangle$ and $|-\rangle$ states, can be induced via the one-exciton to two-exciton transition. We stress that the exciton spin coherence is a direct result of correlations between excitons with opposite spins. In the absence of these correlations, the two-exciton states can be factored into product states of single excitons, the system is reduced to that shown in Fig. 5(a), and no exciton spin coherence can be induced.

Effects of Coulomb correlations on coherent nonlinear optical processes have been investigated extensively in earlier studies and can be described by microscopic theories based on dynamics controlled truncation schemes and also on the use of *N*-exciton many-body eigenstates.[36,41–44,46] These earlier studies have primarily focused on effects of Coulomb correlations in a weakly nonlinear regime. In contrast, EIT can involve nonlinear optical processes to all orders of the pump field, and thus high-order Coulomb correlations are expected to play an even larger role.

### A. Experimental setup

The experimental setup for transient EIT studies was based on a standard transient pump-probe configuration, but with different pump and probe pulse durations. Pump and probe pulses were split from the output of a mode-locked Ti:sapphire laser with a pulse repetition rate of 82 MHz, a spectral bandwidth of 15 meV, and a pulse duration of 150 fs. To obtain the spectrally narrow (and temporally long) pump pulses needed for the experiments, we used an external pulse shaper with which nearly Fourier-transform limited pulses can be obtained. The minimum filtered spectral bandwidth obtained with this setup was $\approx 0.3$ meV. For the experiments presented here, the filtered pump spectral widths were between 0.4 meV and 0.6 meV, with pulse durations of 5–6 ps, as measured by cross correlation with the probe pulses. The probe pulses were unfiltered unless specified otherwise.

The samples studied were (001) GaAs/AlGaAs QW structures grown by molecular-beam epitaxy. Three different structures with well width of 10 nm, 13 nm, and 17.5 nm were used and qualitatively the same results were obtained. For brevity, we present here results obtained from the sample that contains ten periods of 10 nm GaAs well and 10 nm $Al_{0.3}Ga_{0.7}As$ barrier. The GaAs QW samples were held at 10 K in a helium flow cryostat. The samples were etched to remove the GaAs substrate layer, and mounted on sapphire disks for transmission measurements.

The laser spot sizes at the sample were $3\times 10^{-5}$ cm$^2$ for the pump and $4\times 10^{-6}$ cm$^2$ for the probe, so that the probe sampled a region of nearly uniform excitation by the pump. Also, the probe energy flux was kept to less than 1% of the pump. The probe beam transmitted through the sample was collected through a spectrometer with 0.1 meV resolution, and the resulting spectrally resolved signal was detected using a photomultiplier tube. In contrast to many transient pump-probe experiments in which the differential absorption is measured, the magnitude of the nonlinear response was large enough in our experiments so that the full probe absorption was more meaningful. Absorption spectra in the presence or absence of the pump were obtained using $\alpha(\hbar\nu)L=-\ln[I(\hbar\nu)/I_0(\hbar\nu)]$, where $\alpha(\hbar\nu)$ is the absorption coefficient as a function of the probe energy $\hbar\nu$, $L$ is the thickness of the absorbing region of the sample, $I(\hbar\nu)$ is the measured intensity of the probe after passing through the sample, and $I_0(\hbar\nu)$ is the intensity of the probe before pass-

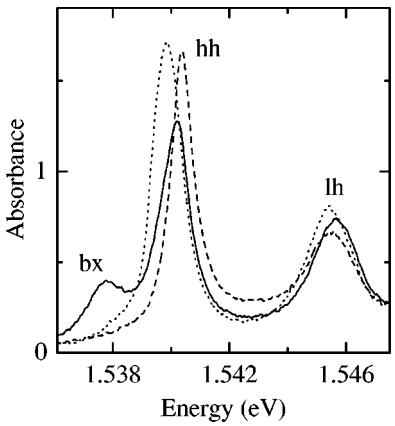


FIG. 6. Absorption spectra in the presence of a $\sigma^+$ prepulse, which is resonant with the hh exciton, has 3 ps duration, and an energy flux of 100 nJ/cm$^2$. The solid (dashed) curve shows the absorption spectrum of a probe which is delayed 10 ps relative to the prepulse and has $\sigma^-$ ($\sigma^+$) polarization. The dotted curve shows the linear absorption spectrum in the absence of the prepulse.

ing through the sample, approximated by measuring the probe spectrum when passed through the sapphire disk only. We will refer to the quantity $\alpha L$ as the absorbance when presenting experimental data.

### B. Spin coherence via bound two-exciton states

As shown schematically in Fig. 5(b), the one-exciton states $|+\rangle$ and $|-\rangle$, and the bound two-exciton state $|+-\rangle_b$ resemble a $\Lambda$-type three-level system. In analogy to the $\Lambda$ system, we apply a strong pump with $\sigma^+$ polarization to the $|-\rangle \leftrightarrow |+-\rangle_b$ transition and a weak probe with $\sigma^-$ polarization to the $|+\rangle \leftrightarrow |+-\rangle_b$ transition. In this configuration, the exciton spin coherence is the nonradiative coherence which can lead to EIT in the optical transition between the one-exciton and bound two-exciton states, i.e., in the biexciton resonance.

Since both of the one-exciton states are initially unoccupied, we prepared an initial population in the $|+\rangle$ state by applying a $\sigma^+$ polarized prepulse with 3 ps duration to the $|+\rangle$ excitonic transition. The prepulse was set to arrive 10 ps before the probe pulse, which is long compared to the exciton dephasing time so that dipole coherences induced by the prepulse do not interfere with the observation of EIT. The 10 ps delay, however, is short compared to the exciton spin relaxation time (50–100 ps),[50] so that only the $|+\rangle$ exciton state is occupied at the start of the EIT experiment. Figure 6 shows the absorption spectra obtained 10 ps after the prepulse (in the absence of the pump). The biexciton absorption resonance corresponding to the $|+\rangle \leftrightarrow |+-\rangle_b$ transition was observed when the probe and the prepulse had the opposite circular polarization. The biexciton resonance vanished when the probe and the prepulse had the same circular polarization.

Figure 7 shows absorption spectra of a $\sigma^-$ probe when both the $\sigma^+$ prepulse and $\sigma^+$ pump were present. The pump was resonant with the $|-\rangle \leftrightarrow |+-\rangle_b$ transition and had an energy flux per pulse of 800 nJ/cm$^2$ (corresponding to a peak

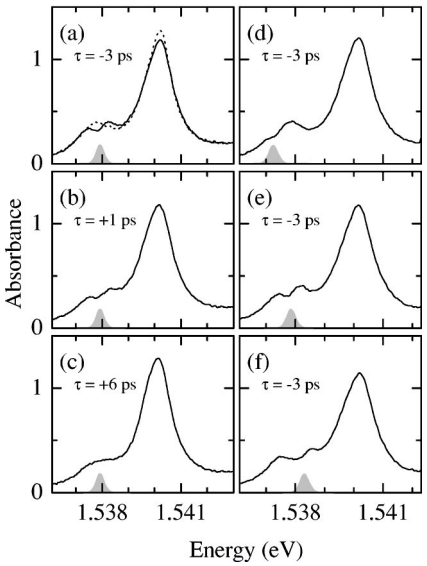


FIG. 7. EIT via bound two-exciton states. Solid curves show the absorption spectra of a $\sigma^-$ probe in the presence of a $\sigma^+$ pump and $\sigma^+$ prepulse. The pump-probe delay is indicated in the figure. The pump spectrum is shown as the shaded area. The dotted curve shows the absorption spectrum in the absence of the pump.

intensity of 150 kW/cm$^2$). The presence of the pump induces a distinct dip in the biexciton absorption resonance. This dip is not due to incoherent spectral hole burning since the pump and probe had opposite circular polarization and also since only the $|+\rangle$ exciton state was populated by the prepulse. As shown in Fig. 7, the absorption dip was most pronounced when the probe arrived 3 ps before the peak of the pump, which is consistent with the expected behavior of EIT in a transient regime as discussed in Sec. II. The dip disappeared when the probe arrived 6 ps after the pump, further confirming that the absorption dip is induced by a coherent process. Figures 7(d)–7(f) show that the spectral position of the dip follows the spectral position of the pump, thus satisfying the characteristic two-photon resonance condition expected for spin coherence in a $\Lambda$-type three-level system.

As discussed above, the polarization configuration for the pump, probe, and prepulse selects a system from the *N*-exciton energy eigenstates which resembles a $\Lambda$ system. The observed temporal and spectral dependence of the absorption dip in the biexciton resonance also shows the characteristics of transient EIT in a $\Lambda$ system, and thus indicates that the dip is due to EIT associated with the exciton spin coherence. However, it should be emphasized that although the EIT resulting from this spin coherence shares similar properties with EIT in an atomic system, the spin coherence itself is the direct result of many-body exciton-exciton correlations. Without these correlations, no coherent superposition of exciton spin states could be induced.

The exciton spin coherence induced in the above experiment is at least to the fourth order of the applied optical fields (including the field of the prepulse), as can be shown by an order-by-order perturbation analysis using the *N*-exciton eigenstates in Fig. 5. Compared with the well-

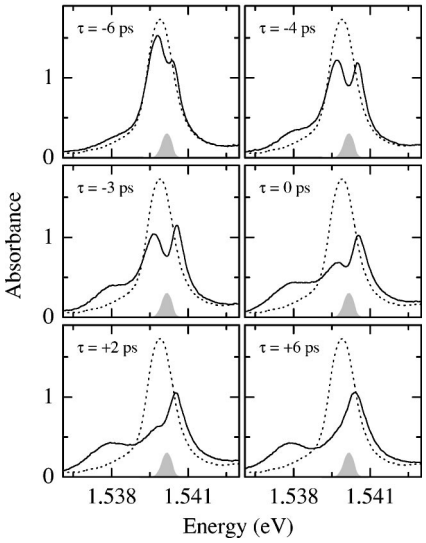


FIG. 8. EIT via unbound two-exciton states. The solid (dotted) curves show the absorption spectra of a $\sigma^-$ probe in the presence (absence) of a $\sigma^+$ pump with energy flux of 400 nJ/cm$^2$. The pump-probe delay is indicated in the figure and the pump spectrum is shown as the shaded area.

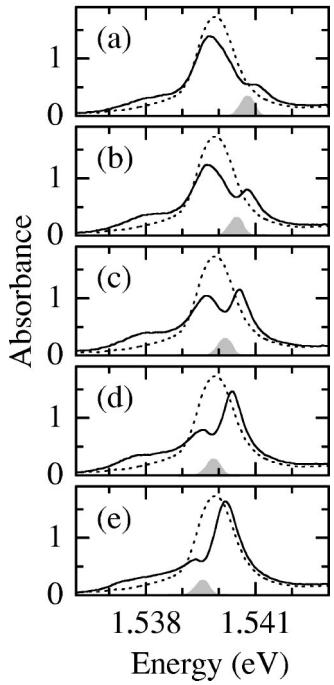


FIG. 9. Dependence of EIT dips on the pump spectral position, with a pump-probe delay $\tau = -3$ ps. Other conditions are the same as for Fig. 8.

known two-exciton coherence, which is to the second order of the applied optical fields and is the result of four-particle Coulomb correlations,[37] the exciton spin coherence can be viewed as due to eight-particle or higher-order Coulomb correlations. Note that theoretical treatment based on the dynamics controlled truncation scheme has thus far been limited to coherences at the level of six-particle Coulomb correlations.[38] Theoretical treatment based on the *N*-exciton eigenstates has thus far been limited to four-particle Coulomb correlations.[42,43] Further theoretical development is still needed for a satisfactory microscopic description of exciton spin coherence and its effects on coherent nonlinear optical responses.

### C. Spin coherence via unbound two-exciton states

As we have discussed above, in addition to the bound two-exciton state, Coulomb interactions between excitons can also lead to a continuum of unbound (but still correlated) two-exciton states. In this section, we explore how these continuum states can be exploited to induce exciton spin coherence and to realize EIT at the exciton resonance. For these experiments, the pump was $\sigma^+$ polarized and was tuned resonant with the exciton transition (no prepulse was used). The absorption spectrum was measured with a $\sigma^-$ polarized probe.

Figure 8 shows the absorption spectra obtained at various pump-probe delays. An absorption dip now occurs at the exciton resonance. The dip becomes visible when the probe precedes the peak of the pump by 6 ps and is the most pronounced when the probe precedes the peak of the pump by 3 ps. The absorption dip becomes strongly asymmetric near the zero pump-probe delay and disappears when the probe arrives after the peak of the pump by only a few picoseconds. The absorption dip is not due to spectral hole burning since the delay dependence in Fig. 8 clearly shows that the dip is due to a coherent process. In fact, aside from the strongly asymmetric spectral line shape near the zero pump-probe delay (which will be discussed in more detail in the following section), the delay dependence is characteristic of the transient EIT process discussed in Sec. II. In Fig. 9 we show that the spectral position of the dip follows almost exactly the spectral position of the pump, indicating the dip satisfies the two-photon resonance condition characteristic of exciton spin coherence.

The above observations of the spectral and temporal response of the absorption dip in the exciton resonance exhibit the characteristics of EIT in a $\Lambda$ system under transient pumping conditions. As was the case for the system involving the bound biexciton state, these observations indicate that the exciton spin coherence is again responsible for the observation of EIT. Furthermore, the properties of the spin coherence and the resulting EIT appear similar whether the spin coherence is induced via the bound or unbound two-excition states.

Figure 10 shows the absorption spectra where we have increased the pump intensity in an effort to increase the degree of transparency. The depth of the EIT dip does not continue to increase for higher pump intensities, but the overall absorption spectrum begins to broaden due to increased decoherence induced by exciton-exciton scattering.

We have also performed experiments under conditions more closely corresponding to the adiabatic conditions typical of EIT experiments in atomic systems. To increase the duration of the probe pulse (and therefore reduce its spectral width), we added a pulse shaper to the probe beam. We obtained the absorption spectrum by scanning the center wave-

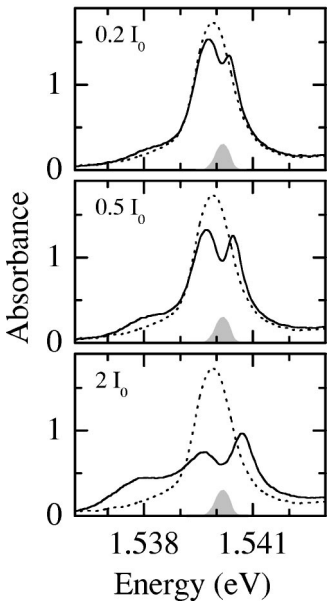


FIG. 10. Dependence of EIT dips on the pump energy flux, with a pump-probe delay $\tau=-3$ ps. The pump energy flux is indicated in the figure, with $I_0=400$ nJ/cm$^2$. The pump spectrum is shown as the shaded area. The dotted curves show the absorption spectrum in the absence of the pump.

length of the probe pulse instead of spectrally resolving the probe pulse after its transmission through the sample. For these measurements, the probe pulse was detected simply with a photodiode, the probe duration was 8 ps, and the pump-probe delay was nominally zero. Figure 11 shows a representative absorption spectrum obtained in this manner, for a pump energy flux of 800 nJ/cm$^2$. The absorption dip is clearly visible but is less pronounced than that obtained in Fig. 8. This is in part due to the fact that the spectral resolution of the above experiment is limited to 0.3 meV, set by the spectral width of the probe pulse. The relatively short duration for the probe is necessary in order to minimize effects of rapid decoherence. In this regard, for systems with short decoherence times, the adiabatic experiments are less desirable as a spectroscopic tool for probing nonradiative coherences than the transient experiments discussed earlier.

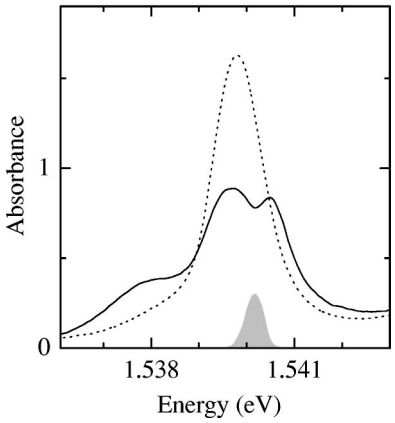


FIG. 11. EIT obtained with a probe of duration of 8 ps and a spectral bandwidth of 0.3 meV. The solid curve shows the absorption spectrum obtained as a function of the center frequency of the probe pulse. The pump-probe delay is zero, and the pump has an energy flux of 800 nJ/cm$^2$. The dotted curve shows the absorption spectrum in the absence of the pump.

It is important to recognize that in the EIT experiments discussed in this section, the $\sigma^+$ polarized pump plays two distinct roles. The first role is to couple to the $|0\rangle\leftrightarrow|+\rangle$ transition. The second role is to couple the $|-\rangle\leftrightarrow|+-\rangle_u$ transition. This second role can be easily overlooked since both of these states are initially unoccupied, but is made apparent by comparison with spin coherence induced via bound two-exciton states. In this case, the coupling of the $|-\rangle$ to $|+-\rangle_u$ states, along with the coupling of the $|+\rangle$ to $|+-\rangle_u$ by the $\sigma^-$ polarized probe pulse, sets up an exciton spin coherence via the unbound two-exciton states. The destructive quantum interference between the polarization induced by the probe and the nonlinear polarization induced by both the pump and exciton spin coherence then leads to the absorption dip observed in the exciton resonance.

Compared with two-exciton coherences associated with unbound two-exciton states, which have been extensively investigated and have been shown to be extremely fragile against exciton-exciton scattering, the spin coherence including that induced via the unbound two-exciton states is relatively robust. This is reflected in the narrow spectral width of the EIT dip shown in Fig. 8. In fact, the width of the observed EIT dip is limited by the spectral width of the pump and not by the decay rate of the spin coherence, except for the dip obtained at the highest pump intensity in Fig. 10. This relative robustness of the exciton spin coherence makes it possible for the high-order Coulomb correlation underlying the exciton spin coherence to have such large effects on the overall optical response. Note that while the exciton spin coherence can be induced via either bound or unbound two-exciton states, the properties of the spin coherence are similar in both cases.

## IV. EXCITON OPTICAL STARK SPLITTING

The EIT line shapes obtained in the above experimental studies display varying degrees of asymmetry, in contrast to what would be expected for an atomic or atomiclike system. The asymmetry depends sensitively on the pump-probe delay and becomes more pronounced as the probe pulse arrives near or after the peak of the pump pulse. While the presence of the lh exciton resonance and the band edge can certainly contribute to the asymmetric spectrum, they cannot account for the observed dynamical changes in the asymmetry. These unusual behaviors, however, can be attributed to effects of exciton energy renormalization, as we discuss in this section.

To better understand the asymmetric EIT line shape and more generally how exciton-exciton interactions affect the temporal evolution of coherent nonlinear optical responses, we have carried out additional experimental studies on exciton optical Stark splitting. Both Rabi oscillations[51] and optical Stark splitting[52] of excitons have been observed in GaAs QW's using transient pump-probe techniques. Our experiments focus on the transient behavior of the optical Stark

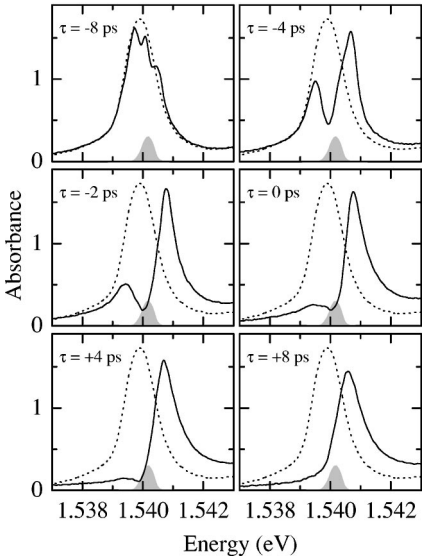


FIG. 12. Dependence of exciton optical Stark splitting on the pump-probe delay. The solid (dotted) curves show the absorption spectra of a $\sigma^+$ probe in the presence (absence) of a $\sigma^+$ pump pulse. The pump energy flux is 400 nJ/cm$^2$, and the pump-probe delay is indicated in the figure. The pump spectrum is shown as the shaded area.

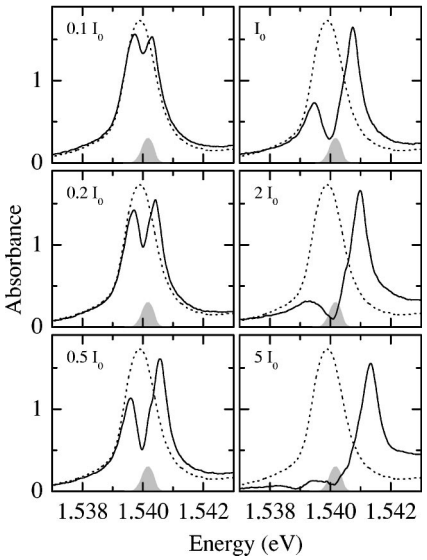


FIG. 13. Dependence of exciton optical Stark splitting on the pump energy flux. The solid (dotted) curves show the absorption spectra of a $\sigma^+$ probe in the presence (absence) of a $\sigma^+$ pump pulse at a pump-probe delay $\tau=-3$ ps. The pump energy flux is indicated in the figure, with $I_0=400$ nJ/cm$^2$. The pump spectrum is shown as the shaded area.

splitting. These experiments were performed in the same manner as the experiments to observe EIT via unbound two-exciton states, except that the pump and probe had the same circular polarization.

Figure 12 shows the absorption spectrum at various pump-probe delays. The Stark splitting first appears when the probe arrives well before the peak of the pump (coherent oscillation[53] in the probe absorption spectrum precedes the appearance of Stark splitting). The splitting initially increases as the delay gets closer to $\tau=0$. The magnitude of the splitting is in general agreement with earlier experiments with comparable pump field amplitudes.[52] Approaching $\tau=0$, however, the splitting becomes more and more asymmetric and harder to discern. When the probe arrives 8 ps after the pump, features related to optical Stark splitting vanish completely. The absorption spectrum now exhibits a large exciton blue shift, along with some saturation of the overall exciton absorption. This confirms that incoherent spectral hole burning plays a negligible role in these measurements (partly due to the fact that the Rabi frequency exceeds the inhomogeneous linewidth). The overall transient behavior of the optical Stark splitting is similar to that of the EIT dip discussed in the preceeding section.

Figure 13 shows the dependence of the optical Stark splitting on the pump intensity where the probe precedes the peak of the pump by a fixed delay of $\tau=-3$ ps. With increasing pumping intensity, the optical Stark splitting increases. However, the Stark splitting also becomes increasingly asymmetric. At the highest pump intensity used, the absorption spectrum is primarily characterized by a large blue shift of the exciton resonance, along with some small features of spectral oscillations.

The dependence of the optical Stark splitting on the pump intensity indicates that the strong asymmetry in the Stark splitting arises from exciton energy renormalization. Resonant generation of excitons by the pump can result in a blue shift of the exciton energy due to exchange interactions between excitons.[54] If we assume that the pump is resonant with the exciton transition in the low excitation limit, with increasing exciton densities the pump becomes increasingly detuned to the lower energy of the actual renormalized exciton resonance, leading to a strong asymmetry in the spectral line shape for the optical Stark splitting. The optical Stark splitting can evolve to an optical Stark shift when the pump is sufficiently detuned from the actual exciton resonance. Note that the induced large blue shift in the exciton resonance can also clamp or limit the exciton density that can be generated by the resonant pump pulse.

For the experiment with a fixed pump-probe delay, increasing the pump intensity results in increasing exciton densities. For the experiment with a fixed pump intensity, moving the probe pulse from the leading edge to the center of the pump also results in an increasing density of excitons that can interact with the polarization induced by the probe pulse. The resulting exciton energy renormalization can account qualitatively for the delay-dependent asymmetric line shape in the transient optical Stark splitting as well as in the transient EIT.

While a detailed microscopic description of the effects of the exciton energy renormalization on optical Stark splitting is beyond the scope of this paper, the much simpler modified optical Bloch equations can provide qualitative guidance for understanding many coherent nonlinear optical phenomena in semiconductors.[34,55] In particular, an exciton blue shift is included in these equations through effects of renormalized

electric fields due to exciton-exciton exchange interactions.[56,57] The effective electric field is given by

$$\mathcal{E}=\mathcal{E}_s+\mathcal{E}_p=\tfrac{1}{2}[E_s(t)e^{i(k_s\cdot r-\nu_s t)}+E_p(t)e^{i(k_p\cdot r-\nu_p t)}+\text{c.c.}] + L\mu(\rho_{eg}+\text{c.c.}), \quad (6)$$

where the $s$ and $p$ subscripts refer to the pump (saturator) and probe fields, respectively, $L$ is the Lorentz local-field factor, and $\rho_{eg}$ and $\mu$ are the off-diagonal density-matrix element and dipole matrix element between the ground and excited states, respectively. In this model, the renormalized electric field leads to a renormalized optical transition energy, with the induced energy shift given by $\hbar\eta n/n_{sat}$, where $\eta=2\mu^2L/\hbar$, $n$ is the exciton density, and $n_{sat}$ is the characteristic exciton saturation density.

For simplicity and to highlight how the exciton blue shift affects the transient behavior of optical Stark splitting, we have included only effects of renormalized electric fields, and neglected effects such as excitation-induced dephasing and additional excitation-induced shifts. We solved the modified optical Bloch equations perturbatively to the first order in the probe field, but keeping all orders of the pump field. We calculated probe absorption spectra for various pump-probe delays and with pump and probe durations of $10\gamma^{-1}$ and $0.1\gamma^{-1}$, respectively. The population relaxation rate for the excited state was $0.01\gamma$ and the pump Rabi frequency was $0.5\gamma$. The left column of Fig. 14 shows the absorption spectra with $\eta=0$. The Stark splitting is the most pronounced for negative pump-probe delays, as expected for this type of coherent transient processes, and all the absorption spectra are symmetric. The right column of Fig. 14 shows the absorption spectra where we took $\eta=2\gamma$. The Stark splitting becomes highly asymmetric as the probe approaches the zero pump-probe delay. The Stark splitting disappears but a blue shift of the transition energy remains when the probe is at the trailing edge of the pump pulse. The above model illustrates qualitatively how the exciton blue shift can lead to unusual transient behaviors similar to those observed in the experiments.

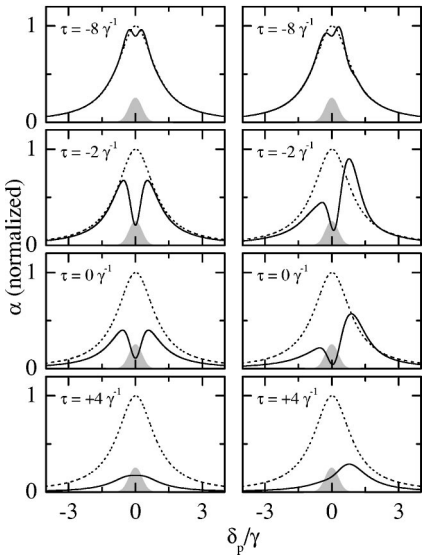


FIG. 14. Theoretical calculation of optical Stark splitting based on the model discussed in the text. The solid (dotted) curves show the absorption spectra of a probe in the presence (absence) of a pump. The pump and probe pulses have durations $10\gamma^{-1}$ and $0.1\gamma^{-1}$, respectively. The pump Rabi frequency is $0.5\gamma$, and the pump-probe delay is indicated in the figure. The left and right columns show the results without and with the Lorentz local-field corrections, respectively.

## V. CONCLUSION

We have demonstrated exciton spin coherence and EIT arising from the exciton spin coherence in the transient optical response in GaAs QWs. The exciton spin coherence is a direct result of Coulomb correlations between excitons with opposite spins and can be induced via the one-exciton to two-exciton (bound or unbound but still correlated) transition. Theoretical analyses based on a simple three-level model, along with additional studies on optical Stark splitting, provide qualitative guidance for understanding the unusual transient behaviors of EIT processes in semiconductors. These analyses also illustrate important conditions for realizing and observing EIT in a transient regime in semiconductors.

The pronounced absorption dip in the $\sigma^+$ exciton resonance induced by coherent resonant excitation of $\sigma^-$ excitons revealed in the EIT experiment provides a striking example on the profound effects of exciton-exciton correlations on coherent nonlinear optical processes, since the $\sigma^+$ and $\sigma^-$ excitonic transitions involved are completely independent of each other in the absence of these correlations. The magnitude of the effect of the exciton spin coherence on the overall optical response underscores the dominant role of high-order (including eight-particle or higher) Coulomb correlations. In this regard, EIT in semiconductors also provides a new avenue for exploring the fascinating interplay between correlations and quantum coherences in an interacting many-particle system.

## ACKNOWLEDGMENTS

This work was supported by ARO/NSA and by NSF under Grants Nos. DMR9733230 and DMR0201784. We thank D. G. Steel and J. E. Cunningham for providing GaAs QW samples used in our study. We are grateful to T. W. Mossberg, V. M. Axt, and R. Binder for many stimulating discussions.

*Present address: Lasers, Optics, and Remote Sensing Department, Sandia National Laboratories, Albuquerque, New Mexico 87185-1423.

[1] M.O. Scully and M.S. Zubairy, *Quantum Optics* (Cambridge University Press, Cambridge, 1997).

[2] E. Arimondo, in *Progress in Optics*, edited by E. Wolf (North-Holland, Amsterdam, 1996), Vol. 35, pp. 259–354.

[3] S.E. Harris, Phys. Today **50(7)**, 36 (1997).

[4] J.E. Field, K.H. Hahn, and S.E. Harris, Phys. Rev. Lett. **67**, 3062 (1991).
[5] K.J. Boller, A. Imamoglu, and S.E. Harris, Phys. Rev. Lett. **66**, 2593 (1991).
[6] S.E. Harris, Phys. Rev. Lett. **62**, 1033 (1989).
[7] A. Imamoglu, J.E. Field, and S.E. Harris, Phys. Rev. Lett. **66**, 1154 (1991).
[8] J. Mompart and R. Corbalán, J. Opt. B: Quantum Semiclassical Opt. **2**, R7 (2000).
[9] J. Oreg, F.T. Hioe, and J.H. Eberly, Phys. Rev. A **29**, 690 (1984).
[10] B.W. Shore, K. Bergmann, J. Oreg, and S. Rosenwaks, Phys. Rev. A **44**, 7442 (1991).
[11] L.V. Hau, S.E. Harris, Z. Dutton, and C.H. Behroozi, Nature (London) **397**, 594 (1999).
[12] M.M. Kash, V.A. Sautenkov, A.S. Zibrov, L. Hollberg, G.R. Welch, M.D. Lukin, Y. Rostovtsev, E.S. Fry, and M.O. Scully, Phys. Rev. Lett. **82**, 5229 (1999).
[13] D.F. Phillips, A. Fleischhauer, A. Mair, R.L. Walsworth, and M.D. Lukin, Phys. Rev. Lett. **86**, 783 (2001).
[14] C. Liu, Z. Dutton, C.H. Behroozi, and L.V. Hau, Nature (London) **409**, 490 (2001).
[15] M.D. Lukin and A. Imamoglu, Nature (London) **413**, 273 (2001).
[16] D.S. Lee and K.J. Malloy, IEEE J. Quantum Electron. **30**, 85 (1994).
[17] Y. Zhao, D.H. Huang, and C.K. Wu, Opt. Lett. **19**, 816 (1994).
[18] M. Lindberg and R. Binder, Phys. Rev. Lett. **75**, 1403 (1995).
[19] G.S. Agarwal, Phys. Rev. A **51**, R2711 (1995).
[20] G.B. Serapiglia, E. Paspalakis, C. Sirtori, K.L. Vodopyanov, and C.C. Phillips, Phys. Rev. Lett. **84**, 1019 (2000).
[21] M.E. Donovan, A. Schulzgen, J. Lee, P.-A. Blanche, N. Peyghambarian, G. Khitrova, H.M. Gibbs, I. Rumyantsev, N.H. Kwong, R. Takayama, Z.S. Yang, and R. Binder, Phys. Rev. Lett. **87**, 237402 (2001).
[22] R. Binder, S.W. Koch, M. Lindberg, N. Peyghambarian, and W. Schäfer, Phys. Rev. Lett. **65**, 899 (1990).
[23] A. Imamoglu and R.J. Ram, Opt. Lett. **19**, 1744 (1994).
[24] M. Phillips and H. Wang, Opt. Lett. **28**, 831 (2003).
[25] M.C. Phillips, H. Wang, I. Rumyantsev, N.H. Kwong, R. Takayama, and R. Binder, Phys. Rev. Lett. **91**, 183602 (2003).
[26] A.A. Belyanin, F. Capasso, V.V. Kocharovsky, V.V. Kocharovsky, and M.O. Scully, Phys. Rev. A **63**, 053803 (2001).
[27] X.D. Hu and W. Poetz, Appl. Phys. Lett. **73**, 876 (1998).
[28] A. Liu and C.Z. Ning, J. Opt. Soc. Am. B **17**, 433 (2000).
[29] L. Silvestri, F. Bassani, G. Czajkowski, and B. Davoudi, Eur. Phys. J. B **27**, 89 (2002).
[30] W.H. Lau, J.T. Olesberg, and M.E. Flatte, Phys. Rev. B **64**, 161301 (2001).
[31] J.A. Gupta, R. Knobel, N. Samarth, and D.D. Awschalom, Science **292**, 2458 (2001).
[32] J. Shah, *Ultrafast Spectroscopy of Semiconductors and Semiconductor Nanostructures*, 2nd ed. (Springer, Berlin, 1999).
[33] D.S. Chemla and J. Shah, Nature (London) **411**, 549 (2001).
[34] H. Wang, K.B. Ferrio, D.G. Steel, Y.Z. Hu, R. Binder, and S.W. Koch, Phys. Rev. Lett. **71**, 1261 (1993).
[35] C. Sieh, T. Meier, F. Janke, A. Knorr, S.W. Koch, P. Brick, M. Hubner, C. Ell, J. Prineas, G. Khitrova, and H.M. Gibbs, Phys. Rev. Lett. **82**, 3112 (1999).
[36] V.M. Axt and A. Stahl, Z. Phys. B: Condens. Matter **93**, 195 (1994).
[37] P. Kner, W. Schäfer, R. Lövenich, and D.S. Chemla, Phys. Rev. Lett. **81**, 5386 (1998).
[38] S.R. Bolton, U. Neukirch, L.J. Sham, D.S. Chemla, and V.M. Axt, Phys. Rev. Lett. **85**, 2002 (2000).
[39] G. Bartels, V.M. Axt, K. Victor, A. Stahl, P. Leisching, and K. Köhler, Phys. Rev. B **51**, 11 217 (1995).
[40] G. Bartels, A. Stahl, V.M. Axt, B. Haase, U. Neukirch, and J. Gutowski, Phys. Rev. Lett. **81**, 5880 (1998).
[41] M. Combescot and R. Combescot, Phys. Rev. Lett. **61**, 117 (1988).
[42] T. Östreich, K. Schönhammer, and L.J. Sham, Phys. Rev. Lett. **74**, 4698 (1995).
[43] T. Östreich, K. Schönhammer, and L.J. Sham, Phys. Rev. B **58**, 12 920 (1998).
[44] V.M. Axt and S. Mukamel, Rev. Mod. Phys. **70**, 145 (1998).
[45] F. Quochi, G. Bongiovanni, A. Mura, J.L. Staehli, B. Deveaud, R.P. Stanley, U. Oesterle, and R. Houdré, Phys. Rev. Lett. **80**, 4733 (1998).
[46] C. Sieh, T. Meier, A. Knorr, F. Jahnke, P. Thomas, and S. Koch, Eur. Phys. J. B **11**, 407 (1999).
[47] G. Chen, N.H. Bonadeo, D.G. Steel, D. Gammon, D.S. Katzer, D. Park, and L.J. Sham, Science **289**, 1906 (2000).
[48] M. Saba, F. Quochi, C. Ciuti, U. Oesterle, J.L. Staehli, B. Deveaud, G. Bongiovanni, and A. Mura, Phys. Rev. Lett. **85**, 385 (2000).
[49] M. Phillips and H. Wang, Phys. Rev. Lett. **89**, 186401 (2002).
[50] T.C. Damen, L. Vina, J.E. Cunningham, J. Shah, and L.J. Sham, Phys. Rev. Lett. **67**, 3432 (1991).
[51] A. Schülzgen, R. Binder, M.E. Donovan, M. Lindberg, K. Wundke, H.M. Gibbs, G. Khitrova, and N. Peyghambarian, Phys. Rev. Lett. **82**, 2346 (1999).
[52] M. Saba, F. Quochi, C. Ciuti, D. Martin, J.L. Staehli, B. Deveaud, A. Mura, and G. Bongiovanni, Phys. Rev. B **62**, R16322 (2000).
[53] B. Fluegel, N. Peyghambarian, G. Olbright, M. Lindberg, S.W. Koch, M. Joffre, D. Hulin, A. Migus, and A. Antonetti, Phys. Rev. Lett. **59**, 2588 (1987), Note that occurences of spectral oscillations in our experiments are greatly reduced due to using a pump pulse with relatively long duration.
[54] N. Peyghambarian, H.M. Gibbs, J.L. Jewell, A. Antonetti, A. Migus, D. Hulin, and A. Mysyrowicz, Phys. Rev. Lett. **53**, 2433 (1984).
[55] H. Wang, K. Ferrio, D.G. Steel, P.R. Berman, Y.Z. Hu, R. Binder, and S.W. Koch, Phys. Rev. A **49**, R1551 (1994).
[56] M. Wegener, D.S. Chemla, S. Schmitt-Rink, and W. Schäfer, Phys. Rev. A **42**, 5675 (1990).
[57] J.M. Shacklette and S.T. Cundiff, Phys. Rev. B **66**, 045309 (2002).